CD4+ Regulatory T Cells Control TH17 Responses in a Stat3-Dependent Manner

Ashutosh Chaudhry, *et al.*

Science **326**, 986 (2009);
DOI: 10.1126/science.1172702

is not equally distributed over the GrIS, but concentrated in the lower accumulation zone. Our model data suggest that over the period 1990–2008, the first 15 m of the firn column in these areas has locally warmed by 5° to >10°. From Fig. 2, B and C, we conclude that, without the moderating effects of increased precipitation and refreezing, the post-1996 cumulative mass anomaly and associated SLR from the GrIS would have been 100% greater than actually observed.

The results also shed light on the relative timing of changes in surface conditions and ice dynamics. In central Greenland, enhanced surface melting started around 1996, several years before marine-terminating glaciers started to accelerate and retreat in the west (~1998) (*6*, *7*) and east (~2002) (*2*, *8*, *10*). In south Greenland, enhanced melting started in the early 1990s, but dynamic thinning was already active south of Helheim glacier in southeast Greenland (*23*, *24*).

To mimic the spatial distribution of GrIS mass loss during the GRACE and ICESat (Ice, Cloud, and Land Elevation Satellite) operational period, we performed a linear regression on 2003–2008 cumulative anomalies of D and SMB components, integrated over five major drainage basins (north, northeast, southeast, southwest, and northwest; fig. S2). The contributions from D and SMB to the basin-integrated mass change are given as numbers in Fig. 3, whereas the contributions from individual SMB components are listed in table S1.

In the north and northeast, which are regions with low accumulation and hence low rates of ice discharge, the discharge anomaly is small, and above-normal runoff dominated 2003–2008 mass loss. In the southwest, the ablation area is relatively large, with few marine-terminating glaciers; here, meltwater production and ice flow strongly interact (*20*–*22*), and increased discharge also contributed to the mass loss. In the northwest, which harbors numerous tidewater glaciers, mass loss is equally distributed between surface processes and ice discharge. In these four basins, surface mass losses represent increased runoff, moderated by above-normal snowfall (table S1).

The greatest 2003–2008 basin mass loss, representing about half of the ice sheet total, is found in the very wet southeast. Here, ice discharge dominates the signal. This is the only basin where the trend in the cumulative precipitation anomaly is negative, after anomalously high snowfall in this region from September 2002 to April 2003 (*25*), just at the onset of the GRACE period. As a result, the surface mass loss in the southeast is equally split between above-normal runoff and below-normal precipitation (table S1). Without the precipitation anomaly, the 2003–2008 mass loss rate in the southeast would have been ~20% smaller.

The colors in Fig. 3 represent surface mass loss rate (2003–2008). Because surface mass loss is dominated by runoff, it is heavily concentrated in the ablation zone of the ice sheet, roughly below 2000 m above sea level (asl). Surface mass loss rates range from 200 to 600 kg m^{-2} $year^{-1}$ in the northern and western ablation zones, and locally exceed 600 kg m^{-2} $year^{-1}$ in the southeast, owing to the effect of decreased precipitation. Assuming (conservatively) the surface mass loss to occur at the density of ice (910 kg m^{-3}), they account for >60 cm $year^{-1}$ of surface lowering locally in the southeast and 20 to 60 cm $year^{-1}$ elsewhere in the GrIS ablation zone. This explains part of the 2003–2008 thinning pattern as observed by the IceSAT and ASTER (Advanced Spaceborne Thermal Emission and Reflection Radiometer) satellites (*26*, *27*), noting that the strong thinning of the fastest-flowing parts of many outlet glaciers, up to several meters per year, remains dominated by dynamic processes. Figure 3 resembles the spatial GrIS mass loss pattern observed by GRACE (*19*), with mass losses concentrated in the southeast, northwest, and southwest at elevations below 2000 m asl.

The good agreement between mass budget calculations and the GRACE data enables us to make a detailed interpretation of the GRACE signal in terms of its individual components. Examining the period with well-constrained discharge data (1996–2008, fig. S4), we see that the ice sheet–integrated GRACE signal primarily consists of (i) the slowly changing ice discharge anomaly, (ii) the asymmetric yet regular sawtooth shape of the seasonal runoff anomaly, and (iii) noise from precipitation variability on monthly to decadal time scales.

References and Notes

1. R. Thomas, E. Frederick, W. Krabill, S. Manizade, C. Martin, *Geophys. Res. Lett.* **33**, L10503 (2006).
2. E. Rignot, P. Kanagaratnam, *Science* **311**, 986 (2006).
3. I. Velicogna, J. Wahr, *Nature* **443**, 329 (2006).
4. J. E. Box, A. E. Cohen, *Geophys. Res. Lett.* **33**, L12706 (2006).
5. E. Hanna *et al.*, *J. Clim.* **21**, 331 (2008).
6. I. Joughin, W. Abdalati, M. Fahnestock, *Nature* **432**, 608 (2004).
7. A. Luckman, T. Murray, *Geophys. Res. Lett.* **32**, L08501 (2005).
8. A. Luckman, T. Murray, R. de Lange, E. Hanna, *Geophys. Res. Lett.* **33**, L03503 (2006).
9. L. A. Stearns, G. S. Hamilton, *Geophys. Res. Lett.* **34**, L05503 (2007).
10. I. M. Howat, I. Joughin, S. Tulaczyk, S. Gogineni, *Geophys. Res. Lett.* **32**, L22502 (2005).
11. I. M. Howat, I. Joughin, T. Scambos, *Science* **315**, 1559 (2007).
12. A. Cazenave, *Science* **314**, 1250 (2006).
13. H. J. Zwally *et al.*, *J. Glaciol.* **51**, 509 (2005).
14. W. Krabill *et al.*, *Science* **289**, 428 (2000).
15. E. Rignot, J. E. Box, E. Burgess, E. Hanna, *Geophys. Res. Lett.* **35**, L20502 (2008).
16. N. L. Bindoff *et al.*, in *Climate Change 2007: The Physical Science Basis* (Cambridge Univ. Press, Cambridge, 2007), pp. 385–432.
17. J. Ettema *et al.*, *Geophys. Res. Lett.* **36**, L12501 (2009).
18. I. Velicogna, *Geophys. Res. Lett.* **36**, L19503.
19. B. Wouters, D. Chambers, E. J. O. Schrama, *Geophys. Res. Lett.* **35**, L20501 (2008).
20. H. J. Zwally *et al.*, *Science* **297**, 218 (2002).
21. R. S. W. van de Wal *et al.*, *Science* **321**, 111 (2008).
22. I. Joughin *et al.*, *Science* **320**, 781 (2008).
23. W. Krabill *et al.*, *Science* **283**, 1522 (1999).
24. E. Rignot, D. Braaten, S. P. Gogineni, W. B. Krabill, J. R. McConnell, *Geophys. Res. Lett.* **31**, L10401 (2004).
25. J. E. Box *et al.*, paper presented at the 8th International Conference on Polar Meteorology and Oceanography, San Diego, CA, 9 to 13 January 2005.
26. D. C. Slobbe, R. C. Lindenbergh, P. Ditmar, *Remote Sens. Environ.* **112**, 4204 (2008).
27. I. M. Howat, B. E. Smith, I. Joughin, T. A. Scambos, *Geophys. Res. Lett.* **35**, L17505 (2008).

28. This work is funded by Utrecht University (M.v.d.B. and W.J.v.d.B.) and the Netherlands Polar Program of the Netherlands Organization of Scientific Research (NWO/ALW) through the international RAPID project (J.E.), UK Natural Environment Research Council grant NE/C509474/1 (J.L.B.), the Royal Netherlands Meteorological Institute (E.v.M.), and Netherlands Institute for Space Research grant SRON/EO-076 (B.W.). E.R. and I.V. performed their work at the University of California, Irvine, and Caltech's Jet Propulsion Laboratory under a contract with NASA's Cryosphere Science Program. Climate data are available from the RAPID data repository at the British Atmospheric Data Centre (badc.nerc.ac.uk).

Supporting Online Material

www.sciencemag.org/cgi/content/full/326/5955/984/DC1
Data and Methods
Figs. S1 to S4
Table S1
References

24 June 2009; accepted 8 September 2009
10.1126/science.1178176

$CD4^+$ Regulatory T Cells Control T_H17 Responses in a Stat3-Dependent Manner

Ashutosh Chaudhry,[1,2] Dipayan Rudra,[1,2] Piper Treuting,[3] Robert M. Samstein,[1] Yuqiong Liang,[1] Arnold Kas,[2] Alexander Y. Rudensky[1,2]*

Distinct classes of protective immunity are guided by activation of STAT transcription factor family members in response to environmental cues. $CD4^+$ regulatory T cells (T_{regs}) suppress excessive immune responses, and their deficiency results in a lethal, multi-organ autoimmune syndrome characterized by T helper 1 (T_H1) and T helper 2 (T_H2) $CD4^+$ T cell–dominated lesions. Here we show that pathogenic T_H17 responses in mice are also restrained by T_{regs}. This suppression was lost upon T_{reg}-specific ablation of Stat3, a transcription factor critical for T_H17 differentiation, and resulted in the development of a fatal intestinal inflammation. These findings suggest that T_{regs} adapt to their environment by engaging distinct effector response–specific suppression modalities upon activation of STAT proteins that direct the corresponding class of the immune response.

The vertebrate immune system affords defense against different classes of pathogens by activation of a particular type of immune response. Intracellular pathogens induce protective T_H1 responses, whereas parasitic helminthes induce T_H2 cytokine production. In contrast, pathogenic yeast, fungi, and extracellular bacteria elicit highly inflammatory T_H17

responses associated with the production of interleukin-17 (IL-17), IL-22, IL-23, and granulocyte recruitment. Commitment of naïve T cells to these effector lineages is influenced by the cues derived from their microenvironment, particularly cytokines. Cytokine receptor signaling results in activation of the STAT (signal transducers and activators of transcription) family of transcription factors. Uncontrolled STAT activation can result in a variety of immune-mediated disease states. For instance, activation of Stat3 in response to the pro-inflammatory cytokine IL-6 in combination with transforming growth factor–β (TGF-β) leads to increased expression of orphan nuclear receptors RORγ and RORα, signature transcription factors for T_H17 cells (*1*–*4*). Deregulated Stat3-dependent T_H17 responses have been implicated in the pathogenesis of inflammatory bowel disease (IBD), psoriasis, multiple sclerosis, and arthritis (*5*).

T_{reg} cells act "in trans" to suppress immune responses to self and to commensal microbiota, and to limit pathology associated with the immune responses to infection. The differentiation and maintenance of suppressive T_{regs} require expression of the X-chromosome–encoded forkhead transcription factor Foxp3 (*6*, *7*). In both humans and mice, mutations in Foxp3 result in a fatal immune disorder characterized by uncontrolled T cell proliferation and drastically elevated production of T_H1 and T_H2 cytokines, suggesting that T_{reg}-elaborated suppression is involved in controlling these responses (*7*). In contrast, T_{reg}-mediated control of T_H17 responses remains an open question. Recent reports suggest that T_H17 and peripherally induced T_{regs} represent competing fates of naïve T cell differentiation, and the lineage choice is determined by relative amounts of IL-6 and TGF-β (*8*–*10*). Therefore, T_{regs} might limit T_H17 differentiation by "stealing" common precursors. Accordingly, a block in T_H17 differentiation in IL-6–deficient mice correlates with an increase in T_{reg} numbers (*11*). We hypothesized that analogous to effector T cell differentiation, T_{regs} suppress a particular type of immune response by activating a distinct STAT family member in response to its cytokine microenvironment. We explored whether activation of Stat3 endows T_{regs} with the ability to suppress T_H17 responses because Stat3 is a key factor in the initiation of T_H17 differentiation.

Using coimmunoprecipitation and Western blot analysis, we found that in T_{regs}, Foxp3 was associated with the transcriptionally active, phosphorylated form of Stat3 (Fig. 1A). Stat3 association with Foxp3 was markedly diminished in cytokine-stimulated T_{regs} cultured in the presence of Stat3 dimerization or phosphorylation inhibitors (fig. S1). These data suggest that Stat3 association with Foxp3 is phosphorylation dependent. In contrast, Stat5, a related STAT family member activated downstream of the IL-2 receptor, did not co-immunoprecipitate with Foxp3 (Fig. 1A).

To assess the role of Stat3 in T_{regs} in vivo, we induced deletion of a conditional *Stat3* allele by crossing $Stat3^{fl/fl}$ mice to $Foxp3^{Cre}$ mice that express a yellow fluorescent protein (YFP)–Cre recombinase fusion protein under the control of the *Foxp3* locus (*12*). We determined that the deletion was efficient and specific to T_{regs} (fig. S2). Male $Foxp3^{Cre}Stat3^{fl/fl}$ and female $Foxp3^{Cre/Cre}Stat3^{fl/fl}$ were born at expected Mendelian ratios and initially appeared healthy. At 6 weeks of age, however, these mice displayed splenomegaly and a pronounced enlargement of the mesenteric lymph nodes (Fig. 1B). In contrast to T_{reg}-deficient mice, we did not observe generalized lymphadenopathy characteristic of a systemic lymphoproliferative disorder. Instead, the size of lymph nodes, except for those draining the gastrointestinal tract, was reduced (Fig. 1B). Over time, $Foxp3^{Cre}Stat3^{fl/fl}$ mice developed anemia, weight loss, rectal prolapse, and colon thickening and succumbed to the disease by 12 to 14 weeks of age (Fig. 1, C and D). These manifestations are hallmarks of IBD, which was further confirmed by histological examination of the intestinal tissue, with the cecum and the colon of the diseased mice exhibiting massive lymphoid and neutrophilic infiltration (Fig. 1, E and F). In addition, hepatitis and liver lipidosis, which are thought to

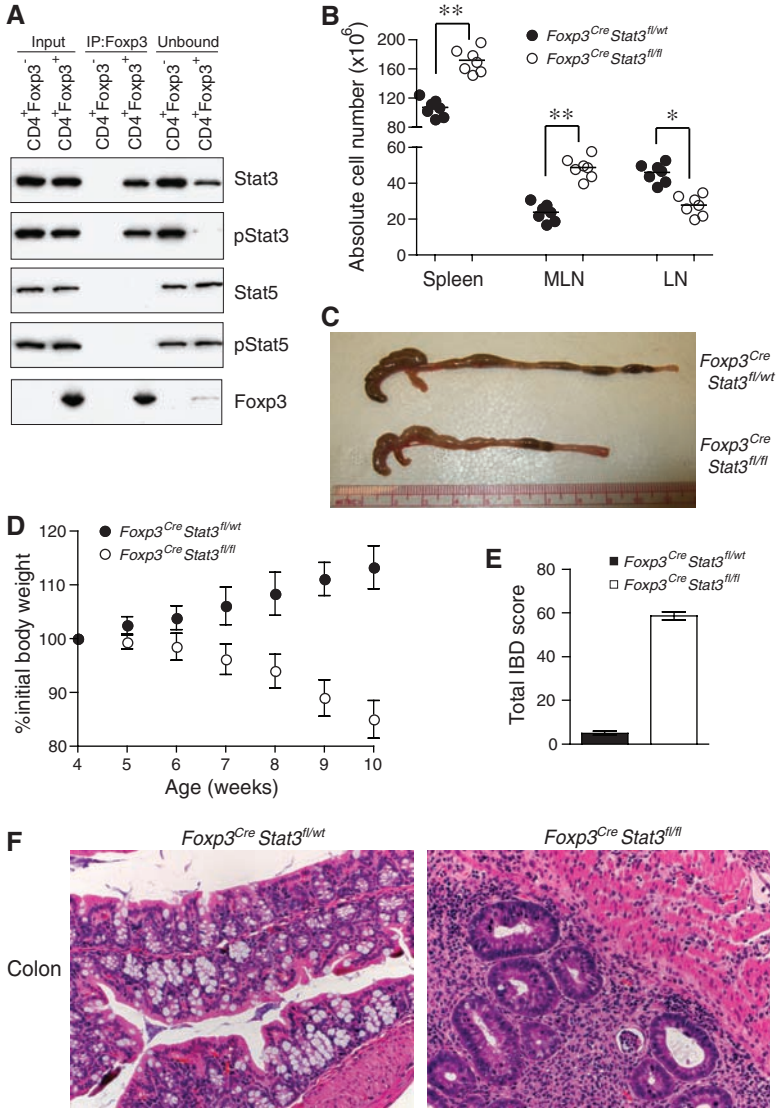

Fig. 1. Phosphorylated Stat3 interacts with Foxp3, and its expression in T_{reg} cells is required for suppression of fatal colitis. (**A**) Foxp3 immunoprecipitation from nuclear lysates of sorted $CD4^+Foxp3^-$ and $CD4^+Foxp3^+$ cells followed by Western blot analysis for the indicated proteins. The input lanes represent 3 to 5% of cell equivalents used for Foxp3 immunoprecipitation. (**B**) Spleen and lymph node cellularity. $^{**}P < 0.001$; $^{*}P < 0.01$. (**C**) Examples of colon thickening. (**D**) Weight loss over time ($n = 7$). (**E**) IBD scores derived from histopathologic evaluation of colon and cecum from 8- to 9-week-old mice. Formalin-fixed sections were stained with hematoxylin and eosin (H&E) before examination ($n = 4$ mice per group). The data in (D) and (E) represent the mean ± SE. (**F**) Representative H&E-stained colon sections from 8- to 9-week-old mice (original magnification, ×20).

[1]Howard Hughes Medical Institute and Immunology Program, Memorial Sloan-Kettering Cancer Center, New York, NY 10065, USA. [2]Department of Immunology, University of Washington, Seattle, WA 98195, USA. [3]Department of Comparative Medicine, University of Washington, Seattle, WA 98195, USA.

*To whom correspondence should be addressed. E-mail: rudenska@mskcc.org

Fig. 2. Stat3 ablation in T_{reg} cells does not affect their numbers, yet leads to $CD4^+$ T cell activation and selective increase in T_H17 responses. (**A**) $CD4^+$ and $CD8^+$ T cell numbers in the spleen and lymph nodes. $^{**}P < 0.001$; $^{*}P < 0.01$. (**B**) Flow cytometric analysis of CD44 and CD62L expression on $CD4^+Foxp3^-$ T cells in 6- to 8-week-old mice. A representative of five independent experiments is shown. (**C**) Frequency and numbers of $CD4^+Foxp3^+$ T cells. $^{**}P < 0.001$; $^{*}P < 0.01$. (**D**) Cytokine production by splenic $CD4^+Foxp3^-$ T cells as determined by flow cytometric analysis. A representative of four independent experiments is shown.

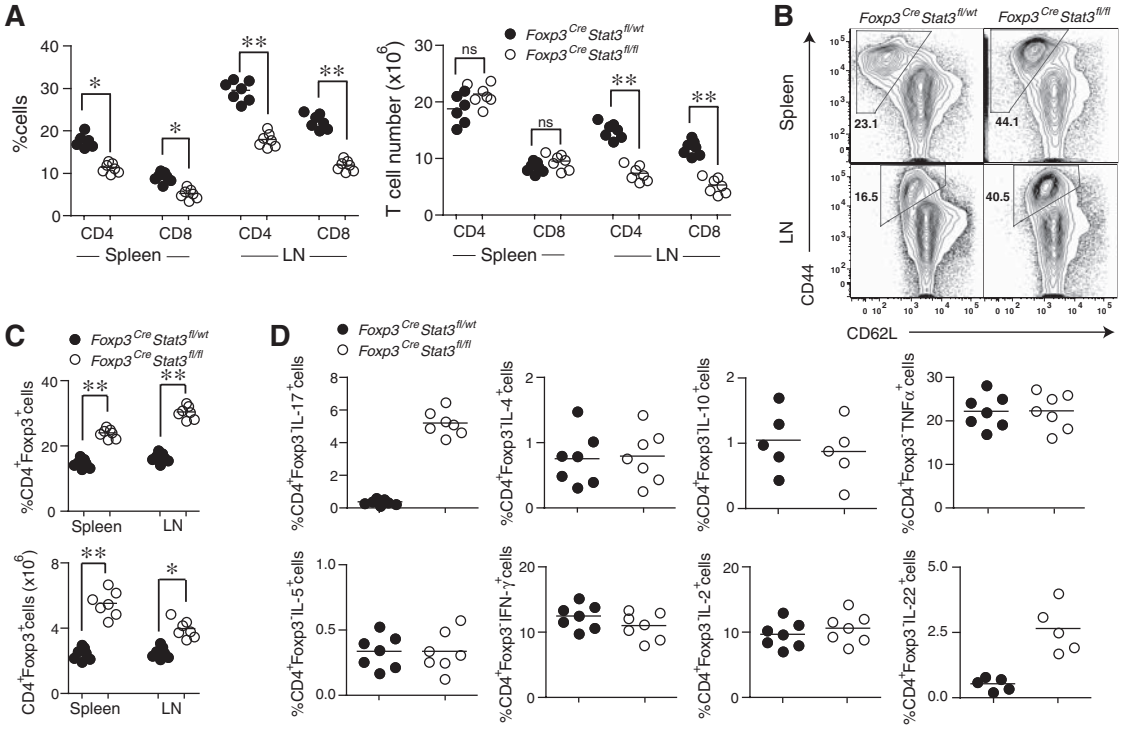

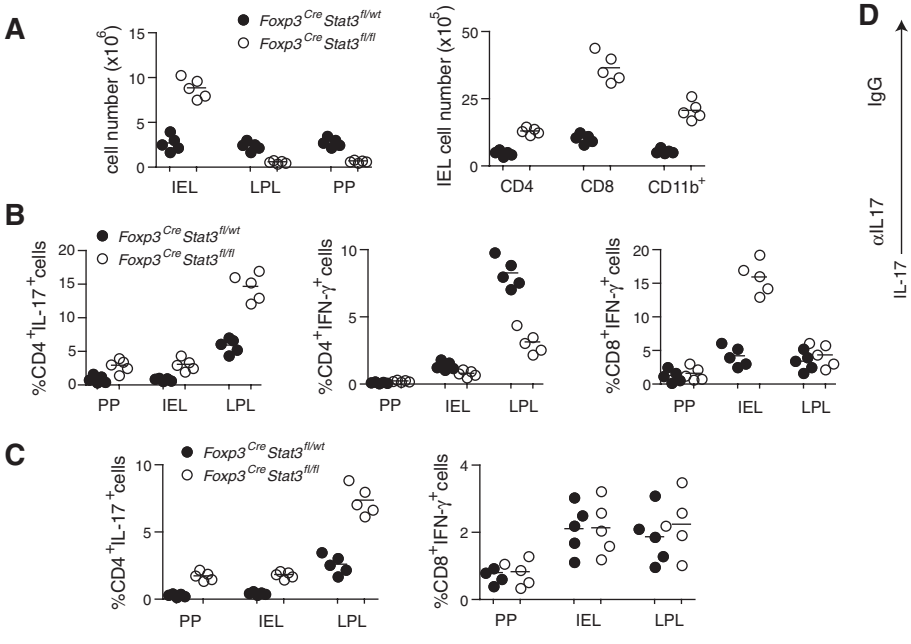

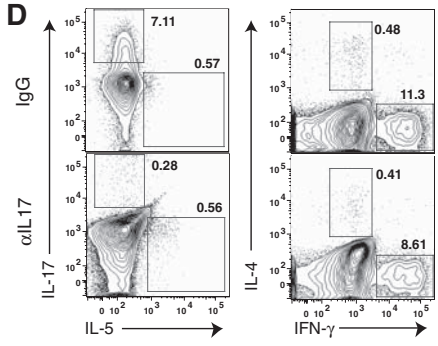

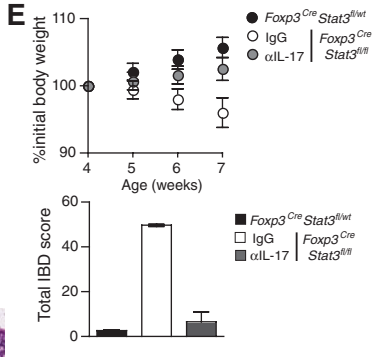

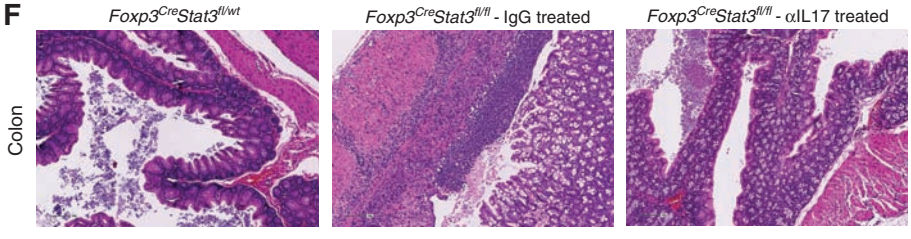

Fig. 3. Increased IL-17 production triggers IBD development in *Foxp3^{Cre}Stat3$^{fl/fl}$* mice. (**A**) Total numbers of PP cells, IELs, and LPLs as well as $CD4^+$, $CD8^+$, $CD11b^+$ cell numbers in the IEL population in 8-week-old mice. (**B**) Frequencies of the indicated cytokine-secreting $CD4^+$ and $CD8^+$ T cells in PP, IEL, and LPL populations in 7- to 8-week-old mice. (**C**) Frequencies of the indicated cytokine-producing $CD4^+$ and $CD8^+$ T cells in PP, IELs, and LPLs in 3- to 4-week-old mice. (**D**) Flow cytometric analysis of cytokine production by splenic $CD4^+Foxp3^-$ T cells in *Foxp3^{Cre}Stat3$^{fl/fl}$* mice treated with isotype-matched immunoglobulin G (IgG) or IL-17 neutralizing antibody. A representative of three independent experiments is shown. (**E**) Weight loss and IBD scores and (**F**) representative H&E-stained colon sections from 7- to 8-week-old *Foxp3^{Cre}Stat3$^{fl/fl}$* mice treated with isotype-matched IgG control or neutralizing IL-17 antibody (original magnification, ×10). The data in (E) represent the mean ± SE.

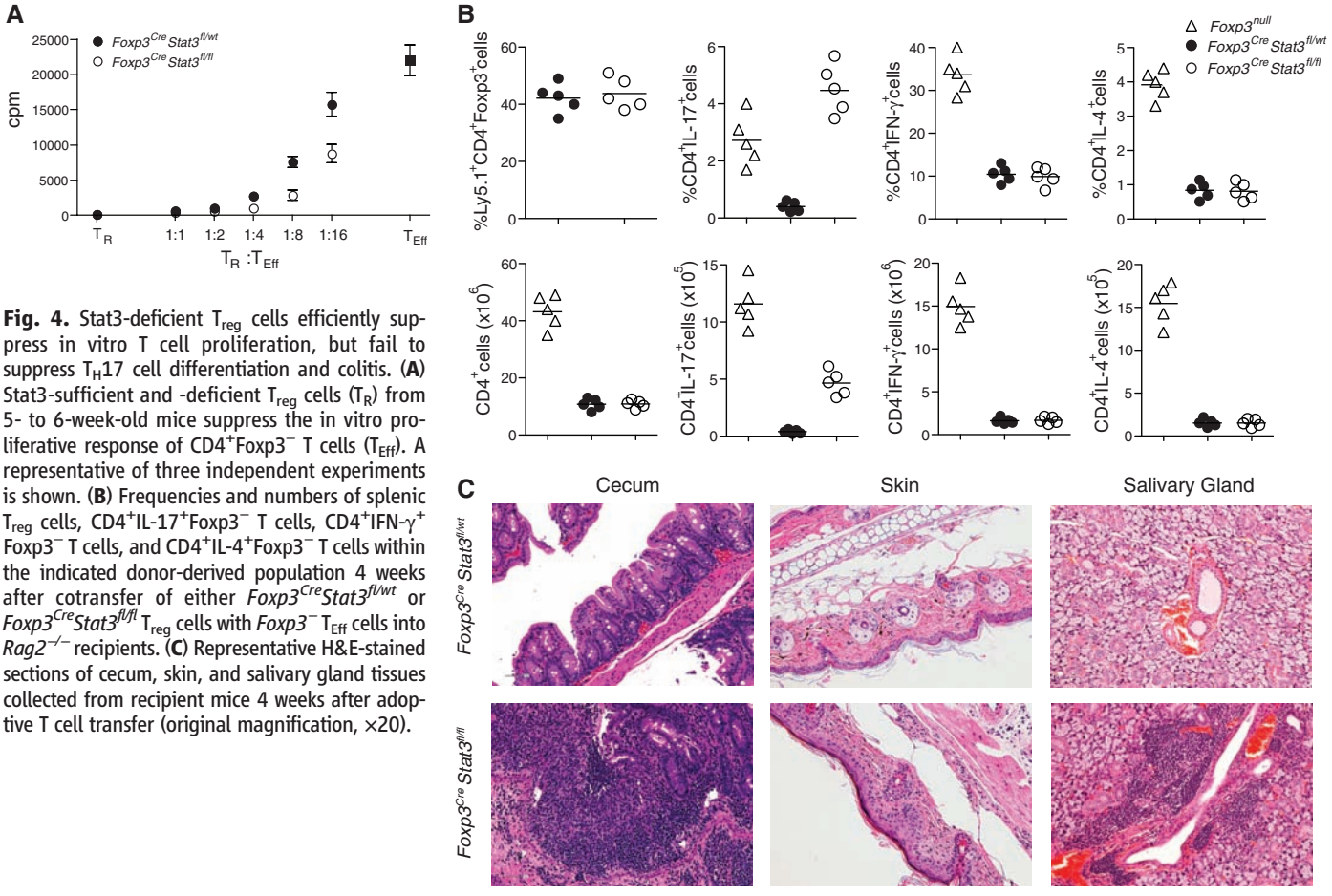

Fig. 4. Stat3-deficient T_{reg} cells efficiently suppress in vitro T cell proliferation, but fail to suppress T_H17 cell differentiation and colitis. (**A**) Stat3-sufficient and -deficient T_{reg} cells (T_R) from 5- to 6-week-old mice suppress the in vitro proliferative response of $CD4^+Foxp3^-$ T cells (T_{Eff}). A representative of three independent experiments is shown. (**B**) Frequencies and numbers of splenic T_{reg} cells, $CD4^+IL\text{-}17^+Foxp3^-$ T cells, $CD4^+IFN\text{-}\gamma^+$ $Foxp3^-$ T cells, and $CD4^+IL\text{-}4^+Foxp3^-$ T cells within the indicated donor-derived population 4 weeks after cotransfer of either *Foxp3*^{Cre}*Stat3*$^{fl/wt}$ or *Foxp3*^{Cre}*Stat3*$^{fl/fl}$ T_{reg} cells with *Foxp3*$^-$ T_{Eff} cells into *Rag2*$^{-/-}$ recipients. (**C**) Representative H&E-stained sections of cecum, skin, and salivary gland tissues collected from recipient mice 4 weeks after adoptive T cell transfer (original magnification, ×20).

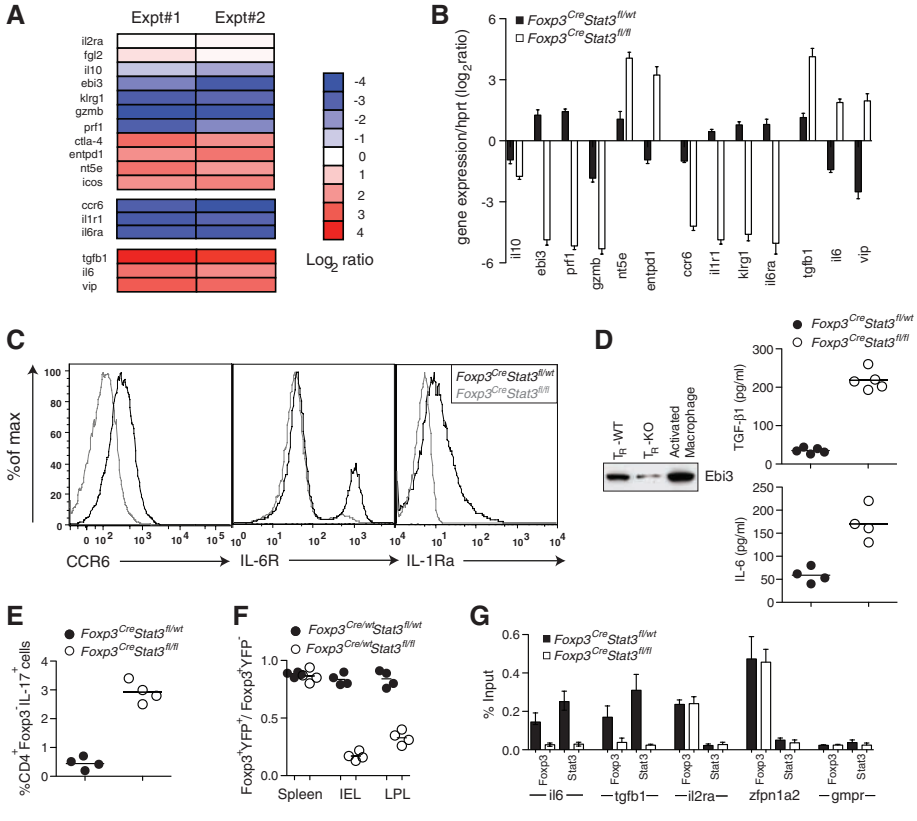

Fig. 5. Stat3-dependent gene expression in T_{reg} cells. (**A** and **B**) Expression pattern of Stat3-dependent genes potentially contributing to T_{reg} suppressor function. The data represent the average of two independent microarray experiments. qPCR analysis of relative expression of the indicated genes in YFP-Cre^+ T_{reg} cells from the indicated mice. The results represent the mean ± SD of relative expression values for the indicated genes relative to hypoxanthine-guanine phosphoribosyl transferase in two independent experiments with three replicates each. (**C**) Flow cytometric analysis of CCR6, IL-1R, and IL-6R expression on T_{regs} from the indicated mice. (**D**) Enzyme-linked immunosorbent assay and Western blot analysis of amounts of TGF-β1, IL-6, and Ebi3 in supernatants of Stat3-sufficient and -deficient T_{regs} cultured in the presence of IL-2. (**E**) $CD4^+Foxp3^-$ were stimulated with antibody to CD3 in the presence of culture supernatants derived from T_{regs} isolated from the indicated mice, and the frequency of $CD4^+IL\text{-}17^+$ cells was assessed by flow cytometry. (**F**) Ratio of $Foxp3^+YFP^+$ to $Foxp3^+YFP^-$ T_{regs} in spleen, IEL and LPL populations of the indicated mice. (**G**) qPCR analysis of Foxp3- and Stat3-bound chromatin isolated from wild-type T_{regs} using the primer set corresponding to the promoter region of the indicated genes. The housekeeping gene *Gmpr* was used as a specificity control. Data represent the mean ± SD.

be secondary to colitis, were also observed (fig. S3). In contrast to the massive widespread tissue lesions observed in *Foxp3*$^{-}$ mice, in *Foxp3*^{Cre}*Stat3*$^{fl/fl}$ mice pathology limited to the intestinal mucosa suggested that the absence of Stat3 only affects a particular subset of T_{reg} functions (fig. S3).

As opposed to the systemic T cell expansion observed in T_{reg}-ablated mice (*13*), we observed reduced splenic and lymph node T cell frequencies in *Foxp3*^{Cre}*Stat3*$^{fl/fl}$ mice, whereas the numbers of B cells, macrophages, and dendritic cells were increased (Fig. 2A and fig. S4). Despite reduced or unchanged numbers of T cells in the lymph node and spleen, we observed a marked increase in activated CD44^{high}CD62^{low}CD4^{+} T cells in these mice as compared to control littermates (Fig. 2B). Increased T_{reg} frequencies suggested, however, that the elevation in activated CD4^{+} T cell numbers was not due to reduced numbers of Stat3-deficient T_{regs} (Fig. 2C). Moreover, examination of the surface phenotype of T_{regs} upon Stat3 ablation indicated the heightened activation of T_{regs} in these mice (fig. S5). Furthermore, we found that Stat3-sufficient and -deficient T_{regs} expressed similar amounts of Foxp3, thus excluding altered Foxp3 expression as an explanation for the pathology in *Foxp3*^{Cre}*Stat3*$^{fl/fl}$ mice (fig. S6).

Recent work suggests that proinflammatory T_H17- and T_H1-associated cytokines have a major impact on colitis development and progression (*14*, *15*). Therefore, we assessed T_H1-, T_H17- and T_H2- associated cytokine production in *Foxp3*^{Cre}*Stat3*$^{fl/fl}$ mice. We observed increased production of T_H17-associated cytokines, IL-17 and IL-22, by splenic CD4^{+}Foxp3^{-} T cells in *Foxp3*^{Cre}*Stat3*$^{fl/fl}$ mice (Fig. 2D and fig. S7). In contrast, T_H1- and T_H2-associated cytokine production was kept in check by Stat3-deficient T_{regs}, as demonstrated by the comparable secretion of interferon-γ (IFN-γ), IL-4, and IL-5 in *Foxp3*^{Cre}*Stat3*$^{fl/fl}$ and littermate control mice. Production of IL-2, tumor necrosis factor–α (TNF-α), and IL-10 was also unaffected (Fig. 2D). Notably, Stat3-deficient Foxp3^{+} T_{regs} did not produce any of these cytokines (fig. S8). These results demonstrate a selective dysregulation of T_H17 responses upon Stat3 ablation in T_{regs} and identify T_{reg}-dependent control of T_H17 responses as an essential component of immune homeostasis.

We further analyzed Peyer's patch (PP), intraepithelial lymphocytes (IELs), and lamina propria lymphocytes (LPLs) because most T_H17 cells in normal mice are induced in the gut-associated lymphoid tissue (GALT) in response to intestinal flora (*16*) and because we observed that the intestinal tract was the major site of inflammation in *Foxp3*^{Cre}*Stat3*$^{fl/fl}$ mice. Whereas the numbers of LPLs and PP cells were diminished, we observed increased numbers of IELs, particularly CD8^{+} T cells and mononuclear cells, in agreement with the massive colonic infiltration revealed by the histopathological evaluation (Fig. 3A). Analysis of cytokine production by PP, LPL, and IEL T cells revealed an increased frequency of IL-17–producing CD4^{+}Foxp3^{-} T cells in *Foxp3*^{Cre}*Stat3*$^{fl/fl}$ mice in comparison to controls, whereas IFN-γ production was reduced (Fig. 3B). Stat3 deficiency did not affect the frequencies of IL-2-, IL-4-, and IL-10-producing cells (fig. S9). We also observed elevated frequencies of IFN-γ–producing CD8^{+} T cells among IELs (Fig. 3B).

We next sought to determine whether IL-17 produced by CD4^{+} T cells or IFN-γ produced by CD8^{+} IELs instigated the disease in *Foxp3*^{Cre}*Stat3*$^{fl/fl}$ mice because both cytokines have been implicated in IBD development (*14*, *15*). We observed clinical symptoms of colitis in *Foxp3*^{Cre}*Stat3*$^{fl/fl}$ mice at about 7 to 8 weeks of age, whereas younger mice were disease-free (fig. S10). Assuming that the cytokine skewing should precede IBD development, we analyzed IL-17 and IFN-γ production in 3- to 4-week-old mice. We observed significantly higher frequencies of IL-17–producing CD4^{+}Foxp3^{-} T cells in the PP, LPL and IEL populations in *Foxp3*^{Cre}*Stat3*$^{fl/fl}$ mice, whereas the frequency of IFN-γ–producing CD8^{+} and CD4^{+} T cells was similar in mutant and control mice (Fig. 3C). These results suggested that IL-17 responses act as the initial trigger of the disease. This was further supported by our finding that antibody-mediated IL-17 blockade in disease-free 3- to 4-week-old *Foxp3*^{Cre}*Stat3*$^{fl/fl}$ resulted in the alleviation of colitis and a reduction in T_H17 frequencies similar to those found in *Foxp3*^{Cre}*Stat3*$^{fl/wt}$ controls (Fig. 3, D to F). In contrast, IFN-γ neutralization failed to prevent or delay colitis in *Foxp3*^{Cre}*Stat3*$^{fl/fl}$ mice (fig. S11). Together, these data suggest that dysregulated T_H17 responses drive colitis induction in *Foxp3*^{Cre}*Stat3*$^{fl/fl}$ mice. Unrestricted T_H17 responses are likely to facilitate the activation or recruitment of IFN-γ–producing CD8^{+} T cells at a later stage of disease progression. This phenomenon mirrors an initial requirement for a T_H17 response to bring T_H1 cells to infected or inflamed tissues (*17*, *18*).

The selective dysregulation of T_H17 responses and aggressive colitis observed in *Foxp3*^{Cre}*Stat3*$^{fl/fl}$ mice suggested that only a distinct aspect of the suppressor program was impaired in Stat3-deficient T_{regs}. Consistent with this assumption, their in vitro suppressor capacity was unaffected (Fig. 4A). To examine suppressor function of these cells in vivo, we cotransferred sorted Stat3-deficient or -sufficient Ly5.2^{+} T_{regs} and effector Ly5.1^{+} CD4 T cells from *Foxp3*$^{-}$ mice into *Rag2*$^{-/-}$ (recombination activating gene 2) recipients. Before transfer, the effector CD4 T cell population was heavily T_H1-skewed and contained ~40% of IFN-γ–producing cells, but few IL-17–producing cells (fig. S12). Similar to unmanipulated *Foxp3*$^{-}$ mice, after 4 to 6 weeks, recipients of *Foxp3*$^{-}$ T cells developed a systemic multi-organ autoimmune syndrome, which was completely abrogated upon cotransfer of Stat3-sufficient T_{regs}. Recipient mice that only received Ly5.1^{+} *Foxp3*$^{-}$ CD4 T cells contained 3- to 5-fold higher frequencies and 15- to 20-fold higher numbers of IFN-γ– and IL-4–producing cells as compared to recipient mice transferred with Ly5.1^{+} *Foxp3*$^{-}$CD4 T cells mixed with either Stat3-deficient or -sufficient T_{regs} (Fig. 4B). In contrast, cotransfer of Stat3-deficient T_{regs} resulted in increased frequencies and absolute numbers of only IL-17–producing Ly5.1^{+} *Foxp3*$^{-}$CD4 T cells (Fig. 4B). A similar trend was observed among LPLs in the recipient mice (fig. S13). These mice also developed a fulminant colitis similar to that seen in *Foxp3*^{Cre}*Stat3*$^{fl/fl}$ mice, as well as pronounced dermatitis and sialoadenitis, whereas other organs remained largely unaffected (Fig. 4C and fig. S13). In control mice, cotransfer of Stat3-sufficient T_{regs} prevented all autoimmune manifestations and tissue pathology. It is noteworthy that all three affected tissues are known targets of T_H17-mediated inflammation. Thus, Stat3-deficient T_{regs} are selectively impaired in their ability to control T_H17 responses in vivo, and this impairment leads to fatal colitis.

To gain insight into the potential mechanisms of Stat3-dependent regulation of T_{reg} function, we compared gene expression patterns in Stat3-deficient and -sufficient YFP^{+} T_{regs} isolated from healthy heterozygous *Foxp3*$^{Cre/wt}$*Stat3*$^{fl/fl}$ and *Foxp3*$^{Cre/wt}$*Stat3*$^{fl/wt}$ female mice. Cross-referencing of the resulting data sets with the previously identified set of Foxp3-dependent genes (*19*) showed that 20% of these genes are also dependent on Stat3 expression in T_{regs} (fig. S14). Within this group, we found decreased expression of *Il10*, *Ebi3*, *Gzmb*, and *Prf1*, genes implicated in T_{reg} suppressor function (Fig. 5, A and B). In particular, T_{reg} production of IL-10 and the Ebi3-containing cytokine, IL-35, is important for preventing colitis (*12*, *20*). In contrast, expression of other genes encoding proteins related to T_{reg} suppressor function was unaltered (*Il2ra*, *Fgl2*) or markedly increased (*Ctla4*, *Nt5e*, *Entpd1*, *Tgfb1*).

Substantially reduced expression of *Ccr6* in Stat3-deficient T_{regs} (Fig. 5, A to C) may also contribute to failure of Stat3-deficient T_{regs} to suppress T_H17-mediated inflammation. CCR6 is expressed by both T_H17 and T_{regs} and plays an important role in migration of T_H17 cells to inflammatory sites and in T_{reg}-mediated suppression thereof (*21*, *22*). We therefore compared relative distribution of YFP-Cre^{+} Stat3-deficient and YFP-Cre^{-} Stat3-sufficient Foxp3^{+} T_{regs} in the colon, secondary lymphoid organs, and GALT in the absence of any inflammation in female heterozygous *Foxp3*$^{Cre/wt}$Stat3$^{fl/fl}$ mice. These cells were present at a ~1:1 ratio in spleen; however, we observed a diminished proportion of Stat3-deficient T_{regs} in the gut (Fig. 5E). These results are consistent with the idea that Stat3-deficient T_{reg} cells are impaired in their ability to migrate to the gut tissue before establishment of colitis because Stat3-deficient and -sufficient T_{reg} cell populations had similar proportions of cycling and apoptotic cells (fig. S15). In contrast to healthy *Foxp3*$^{Cre/wt}$Stat3$^{fl/fl}$ mice, increased numbers of Foxp3^{+} T cells were observed in the inflamed colon of *Foxp3*^{Cre}Stat3$^{fl/fl}$ mice, in agreement with a recent report that CCR6-deficient T cells enter the central nervous system at late, but not at early, stages in the progression of experimental autoimmune encephalomyelitis (*18*).

Additionally, a low level of IL-1 receptor and IL-6 receptor expression in Stat3-deficient T_{regs}

(Fig. 5C) can potentially reduce the ability of these receptors to compete with effector T cells and other immune cell types for IL-1 and IL-6, cytokines that enhance T_H17 differentiation (*3*, *10*, *23*). In this regard, IL-2 receptor expressed on T_{regs} can deprive effector T cells of IL-2, thereby, effectively limiting the immune response (*24*). Consistent with this idea, Stat3-sufficient, but not Stat3-deficient, T_{regs} depleted IL-1 and IL-6 from the culture medium (fig. S17).

Unexpectedly, Stat3 deficiency in T_{regs} resulted in increased expression of *Il6*, *Tgfb1*, and *Vip*. Although T_{reg}-produced TGF-β1 can mediate suppression (*25*), TGF-β1 in combination with IL-6 also facilitates the generation of T_H17 cells. Similarly, *Vip*-encoded vasoactive intestinal peptide (VIP) promotes T_H17 differentiation (*26*). Indeed, soluble factors produced by Stat3-deficient T_{regs} facilitated differentiation of IL-17–producing T cells in vitro in the absence of exogenously supplied IL-6 and TGF-β1 (Fig. 5F). Increased expression of IL-6 and TGF-β1 in Stat3-deficient T_{regs} (Fig. 5, B and D) might amplify, but cannot fully account for, the observed increase in IL-17 production in diseased $Foxp3^{Cre}Stat3^{fl/fl}$ mice because heterozygous $Foxp3^{Cre/wt}Stat3^{fl/fl}$ female mice cohabited by Stat3-deficient and -sufficient T_{regs} do not exhibit augmented T_H17 responses.

To test whether Stat3 facilitates recruitment of Foxp3 to regulatory elements of *Il6* and *Tgfb1* genes, we used chromatin immunoprecipitation combined with quantitative polymerase chain reaction (qPCR) to examine Foxp3 binding to promoter regions of these genes in Stat3-sufficient and -deficient T_{reg} cells. Indeed, we found that Foxp3 was bound to *Il6* and *Tgfb1* promoters in a Stat3-dependent manner. In contrast, Foxp3 binding to *Zfpn1a2* (Helios) and *Il2ra*, well-known Foxp3-binding genes expressed in a Stat3-independent manner, was unaffected by the absence of Stat3 (Fig. 5G). These results suggest that Stat3 activation–dependent association with Foxp3 transcriptional complexes may result in modulation of Stat3-dependent gene expression partly through Stat3-dependent recruitment of Foxp3.

Thus, the activation of Stat3 in T_{regs} endows them with the ability to suppress T_H17 responses plausibly through increased expression of a subset of suppressor molecules, as well as cytokine and chemokine receptors, which may deprive immune effector cells of essential activation cues and facilitate the spatial proximity of T_{regs} and T_H17 cells. Furthermore, Stat3 in T_{regs} limits the expression of soluble mediators of T_H17 differentiation. We suggest that altered expression of a combination of genes, but not changes in any one of them, can account for the inability of Stat3-deficient T_{regs} to restrain T_H17 responses.

Our findings support the idea that the same transcription factors integrate environmental cues that guide a particular immune response type and facilitate T_{reg} cells' ability to suppress the corresponding type of immune response. Consistent with this notion, Irf4 (interferon regulatory factor 4), an IRF transcription factor family member essential for T_H2 differentiation, is required for T_{reg} cells to suppress T_H2 responses (*27*). Furthermore, T_{reg} expression of T-bet, a T_H1-specific transcription factor, is required for T_{reg} homeostasis under conditions of induced T_H1 inflammation (*28*). We propose that the STAT-IRF axis of transcriptional regulation allows T_{regs} to adapt to a particular environment and ensures appropriate "class"-specific control of immune-mediated inflammation.

References and Notes

1. P. R. Mangan *et al.*, *Nature* **441**, 231 (2006).
2. M. Veldhoen, R. J. Hocking, C. J. Atkins, R. M. Locksley, B. Stockinger, *Immunity* **24**, 179 (2006).
3. L. Zhou *et al.*, *Nat. Immunol.* **8**, 967 (2007).
4. X. O. Yang *et al.*, *Immunity* **28**, 29 (2008).
5. E. Bettelli, T. Korn, M. Oukka, V. K. Kuchroo, *Nature* **453**, 1051 (2008).
6. S. Hori, T. Nomura, S. Sakaguchi, *Science* **299**, 1057 (2003).
7. J. D. Fontenot, M. A. Gavin, A. Y. Rudensky, *Nat. Immunol.* **4**, 330 (2003).
8. I. I. Ivanov *et al.*, *Cell* **126**, 1121 (2006).
9. E. Bettelli *et al.*, *Nature* **441**, 235 (2006).
10. L. Zhou *et al.*, *Nature* **453**, 236 (2008).
11. T. Korn *et al.*, *Nature* **448**, 484 (2007).
12. Y. P. Rubtsov *et al.*, *Immunity* **28**, 546 (2008).
13. J. M. Kim, J. P. Rasmussen, A. Y. Rudensky, *Nat. Immunol.* **8**, 191 (2007).
14. W. Strober, I. J. Fuss, R. S. Blumberg, *Annu. Rev. Immunol.* **20**, 495 (2002).
15. K. J. Maloy, M. C. Kullberg, *Mucosal Immunol.* **1**, 339 (2008).
16. I. I. Ivanov *et al.*, *Cell Host Microbe* **4**, 337 (2008).
17. S. A. Khader *et al.*, *Nat. Immunol.* **8**, 369 (2007).
18. A. Reboldi *et al.*, *Nat. Immunol.* **10**, 514 (2009).
19. M. A. Gavin *et al.*, *Nature* **445**, 771 (2007).
20. D. A. Vignali, L. W. Collison, C. J. Workman, *Nat. Rev. Immunol.* **8**, 523 (2008).
21. M. Kleinewietfeld *et al.*, *Blood* **105**, 2877 (2005).
22. T. Yamazaki *et al.*, *J. Immunol.* **181**, 8391 (2008).
23. C. Sutton, C. Brereton, B. Keogh, K. H. Mills, E. C. Lavelle, *J. Exp. Med.* **203**, 1685 (2006).
24. P. Pandiyan, L. Zheng, S. Ishihara, J. Reed, M. J. Lenardo, *Nat. Immunol.* **8**, 1353 (2007).
25. M. O. Li, Y. Y. Wan, R. A. Flavell, *Immunity* **26**, 579 (2007).
26. M. Yadav, J. Rosenbaum, E. J. Goetzl, *J. Immunol.* **180**, 2772 (2008).
27. Y. Zheng *et al.*, *Nature* **458**, 351 (2009).
28. M. A. Koch *et al.*, *Nat. Immunol.* **10**, 595 (2009).

29. We thank K. Forbush, T. Chu, L. Karpik, and A. Bravo for assistance with the mouse colony management; S. Akira for *Stat3*$^{fl/fl}$ mice; and J. Renauld for antibody to IL-22. This work was supported by NIH grants AI-061816 and AI-034206. A.C. is supported by the Cancer Research Institute, and D.R. is supported by the Arthritis Foundation. A.Y.R. is an investigator with the Howard Hughes Medical Institute. Gene expression microarray data have been deposited in the NCBI Gene Expression Omnibus repository with the accession code GSE17962.

Supporting Online Material

www.sciencemag.org/cgi/content/full/1172702/DC1
Methods
Figs. S1 to S17
References

24 February 2009; accepted 2 September 2009
Published online 1 October 2009;
10.1126/science.1172702
Include this information when citing this paper.

A Spindle Assembly Checkpoint Protein Functions in Prophase I Arrest and Prometaphase Progression

Hayden Homer,* Liming Gui, John Carroll

Two critical stages of mammalian oocyte regulation are prophase I arrest, which is important for sustaining the oocyte pool, and the progression through meiosis I (MI) to produce fertilizable eggs. We have found that the spindle assembly checkpoint protein BubR1 regulates both stages in mouse oocytes. We show that oocytes depleted of BubR1 cannot sustain prophase I arrest and readily undergo germinal vesicle breakdown, a marker for reentry into MI. BubR1-depleted oocytes then arrest before completing MI, marked by failure of polar body extrusion. Both meiotic defects in BubR1-depleted oocytes are due to reduced activity of the master regulator known as the anaphase-promoting complex (APC), brought about through diminished levels of the APC coactivator Cdh1.

Mammalian oocytes arrest at prophase I from birth until puberty when hormonal signals induce the resumption of meiosis I (MI) and progression to meiosis II (MII), the stage at which fertilization occurs. Prophase I–arrested oocytes possess an intact nucleus referred to as the germinal vesicle (GV), with GV breakdown (GVBD) and first polar body extrusion (PBE) signifying the resumption and conclusion of MI, respectively (Fig. 1A). Cell-cycle progression is driven by a proteolytic machinery known as the anaphase-promoting complex (APC) acting in concert with one of two coactivators, Cdc20 or Cdh1 (*1*). Unlike mitotic prometaphase—in which APC-Cdc20 is the principal APC species (*1*)—in mammalian oocytes, APC-Cdh1 is active during prophase I (*2*, *3*) and early prometaphase I before APC-Cdc20, which acts in late MI (*4*) (Fig. 1A). In both systems, however, the anaphase-trigger is APC-Cdc20–mediated securin and cyclin B1 degradation (*1*, *4*, *5*). The key inhibitor of APC-Cdc20–dependent anaphase onset is the spindle assembly checkpoint (SAC), the core compo-

Oocyte and Embryo Research Laboratory, Department of Cell and Developmental Biology, Division of Biosciences and Institute for Women's Health, University College London, London, UK.

*To whom correspondence should be addressed. E-mail: h.homer@ucl.ac.uk